

EUIS-Net: A Convolutional Neural Network for Efficient Ultrasound Image Segmentation

Shahzaib Iqbal¹[0000–1111–2222–3333], Hasnat Ahmed¹, Muhammad Sharif¹, Madiha Hena², Tariq M. Khan³, and Imran Razzak³

¹ Department of Electrical Engineering, Abasyn University Islamabad Campus(AUIC), Islamabad, Pakistan (shahzeb.iqbal@abasynisb.edu.pk)

² Department of Computing, Abasyn University Islamabad Campus(AUIC), Islamabad, Pakistan (madiha.hena@abasynisb.edu.pk)

³ School of Computer Science & Engineering, UNSW, Sydney, Australia {tariq.khan, imran.razzak}@unsw.edu.au

Abstract. Segmenting ultrasound images is critical for various medical applications, but it offers significant challenges due to ultrasound images’ inherent noise and unpredictability. To address these challenges, we proposed EUIS-Net, a CNN network designed to segment ultrasound images efficiently and precisely. The proposed EUIS-Net utilises four encoder-decoder blocks, resulting in a notable decrease in computational complexity while achieving excellent performance. The proposed EUIS-Net integrates both channel and spatial attention mechanisms into the bottleneck to improve feature representation and collect significant contextual information. In addition, EUIS-Net incorporates a region-aware attention module in skip connections, which enhances the ability to concentrate on the region of the injury. To enable thorough information exchange across various network blocks, skip connection aggregation is employed from the network’s lowermost to the uppermost block. Comprehensive evaluations are conducted on two publicly available ultrasound image segmentation datasets. The proposed EUIS-Net achieved mean IoU and dice scores of 78.12%, 85.42% and 84.73%, 89.01% in the BUSI and DDTI datasets, respectively. The findings of our study showcase the substantial capabilities of EUIS-Net for immediate use in clinical settings and its versatility in various ultrasound imaging tasks.

Keywords: Ultrasound Images · Breast Cancer Lesion Segmentation · Convolutional Neural Network · Medical Image Segmentation

1 Introduction

Breast cancer remains a prevalent disease and a leading cause of mortality among women worldwide, as highlighted by the World Health Organisation (WHO) [1]. In 2020, breast cancer alone accounted for 2.3 million new cases and 685,000 deaths worldwide [2]. Projections indicate that by 2040, these numbers could reach more than 3 million new cases and approximately 1 million deaths annually [3]. Various imaging modalities, including mammography, computed tomography (CT), magnetic resonance imaging (MRI), and breast ultrasound (BUS), play crucial roles in breast cancer detection. Mammography, the standard diagnostic tool, has limitations due to its use of ionising radiation, making it unsuitable for pregnant women [4]. In contrast, BUS imaging

is both cost-effective and radiation-free, making it an invaluable screening tool [5]. It provides detailed information on the characteristics of breast tissue and the presence of malignant tissues [5].

Segmentation of breast lesions from ultrasound images has been extensively investigated using various algorithms. These methods can be broadly categorised into early techniques and machine learning approaches [6]. Early techniques include methods such as graph-based models, region-growing models, and deformable models. Machine learning approaches encompass traditional hand-made methods and more recent deep learning (DL) techniques [7–10].

Graph-based models optimise energy using frameworks like Markov random fields or graph cuts. Chiang et al. [11] employed a pre-trained Probabilistic Boosting Tree (PBT) classifier to compute the data term within graph-cut energy, while Xian et al. [12] integrated information from both frequency and spatial domains to formulate the energy function. However, these models may struggle to capture intricate semantic features and delineate faint boundaries in low-contrast ultrasound images, leading to inaccuracies.

Deformable models start with an initial representation and iteratively deform toward object boundaries, guided by internal and external energy factors. For example, Madabhushi et al. [13] used boundary points and balloon forces to define the external energy in their deformable model. Chang et al. [13] reduced speckle noise in ultrasound images using a stick filter and applied a discrete 3D active contour model to accurately segment regions of breast lesions by deforming the model.

Region-growing methods initiate segmentation by starting from manually or automatically selected seed points and gradually expanding to delineate target region boundaries based on predefined growth criteria. Shan et al. [14] used this approach to segment breast cancer, incorporating criteria such as contour smoothness and region similarity to enhance the segmentation process.

Machine learning-based approaches have traditionally relied on hand-crafted features to train classifiers for segmentation tasks [15–17]. In contrast, recent advances in deep learning, particularly convolutional neural networks (CNN), have shown promise in automatically learning high-level features from data [18–20]. For example, models such as ESTAN [21], RCA-IUnet [22], CTG-Net [23], and BGM-Net [24] have been developed specifically for breast tumour segmentation in ultrasound images. These models incorporate innovations such as attention mechanisms, multiscale features, and boundary-guided networks to improve segmentation accuracy.

Despite progress, current methods still face significant challenges. Region-growing methods are hindered by noise and variable tissue properties, while graph models often fail to capture complex tumor features in low-contrast images. Deformable models are highly sensitive to initialisation, leading to suboptimal results depending on the starting conditions. Handcrafted feature approaches may not fully exploit the extensive information present in the data. Although deep learning methods are promising, they require further refinement to enhance segmentation accuracy.

To address these challenges, we proposed EUIS-Net, a CNN network optimized for efficient and precise ultrasound image segmentation. EUIS-Net employs four encoder-decoder blocks, significantly reducing computational complexity while maintaining exceptional performance. The network integrates both channel and spatial attention mech-

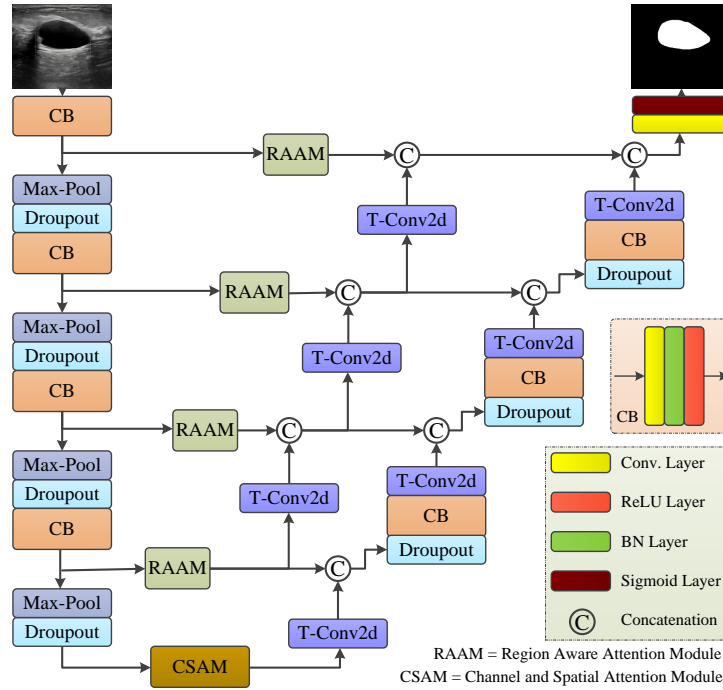


Fig. 1: Schematic of the proposed method.

anisms in the bottleneck to enhance feature representation and capture critical contextual information. In addition, it incorporates a region-aware attention module (RAAM) into the skip connections, improving the focus on the areas of the injury. To ensure comprehensive information exchange across different network blocks, skip connection aggregation is used from the lowest to the highest block.

The remainder of this manuscript is structured as follows. Section 2 details the architecture of the proposed EUIS-Net model. Section 3 presents the experimental results and discussions. Finally, Section 4 concludes the paper and outlines potential future research directions.

2 Proposed Method

In this section, the proposed EUIS-Net is discussed briefly. The proposed EUIS-Net starts with a feature extraction block that employs a convolutional block (CB) followed by a max-pooling operation and a dropout layer. The encoder of the proposed EUIS-Net uses four feature extraction blocks. Once feature information is extracted on multiple spatial scales, these features are further refined by channel and spatial attention modules at the bottleneck layer. The proposed EUIS-Net decoder uses the same convolutional

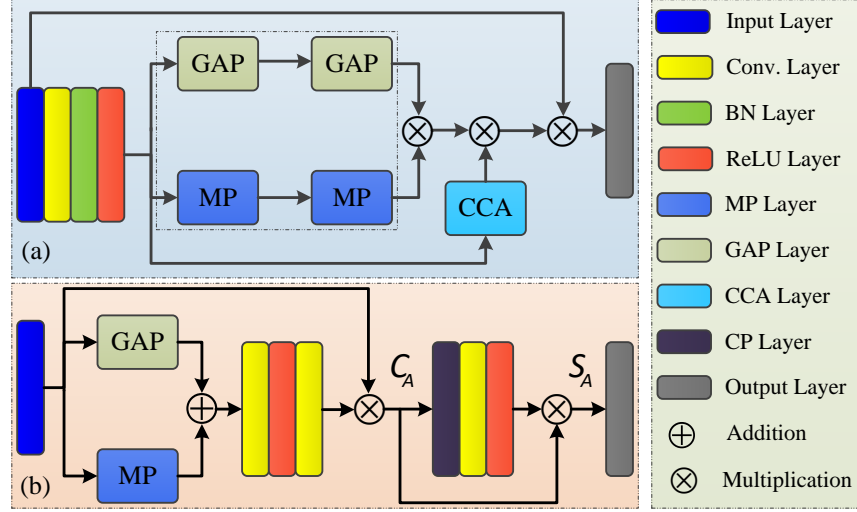


Fig. 2: Schematic of the attention modules: (a) region aware attention module, (b) channel and spatial attention module.

blocks to reconstruct the feature maps in their actual spatial dimension. The proposed method also uses region-aware attention modules [16] in the skip connection to refine and control the feature information flow between the encoder and decoder blocks.

Let In be the RGB image given as input to the proposed method. The output of the first encoder block (B_E^1) is computed by applying a convolutional block (CB) on the input as given in (Eq. 1).

$$B_E^1 = CB(In) \quad (1)$$

where CB is the convolutional block that uses the standard convolutional operation followed by a batch normalisation layer and activation function computed in (Eq.2).

$$CB = \Re(B_n(f^{3 \times 3}(In))) \quad (2)$$

where $(f^{3 \times 3})$ is the standard convolutional operation with a kernel size of (3×3) , B_n is the batch normalization and \Re is the ReLU activation layer. The output of the 2^{nd} , 3^{rd} and 4^{th} encoder blocks are computed as (Eqs. 3–5).

$$B_E^2 = CB(D_r(M_p(B_E^1))) \quad (3)$$

$$B_E^3 = CB(D_r(M_p(B_E^2))) \quad (4)$$

$$B_E^4 = CB(D_r(M_p(B_E^3))) \quad (5)$$

where (D_r) is the dropout layer and (M_p) is the max-pooling operation. Once the feature information is extracted, it is refined by the channel and spatial attention module (CSAM). The output of the 1st decoder block (B_D^1) is calculated employing a max-pooling operation followed by dropout, CSAM, and transposed convolution (for up-sampling) on the 4th encoder block (B_E^4) and then concatenating it with the output of the region-aware attention module (RAAM) applied on the encoder block 4th (B_E^4) as computed in (Eq. 6).

$$B_D^1 = [f_t^{3 \times 3} (\text{CSAM} (D_r (M_p (B_E^4))))] \odot [\text{RAAM} (B_E^4)] \quad (6)$$

where $f_t^{3 \times 3}$ is the transposed convolution operation with a kernel size of (3×3) and \odot is the concatenation operation. The output of the 2nd, 3rd and 4th decoder blocks are computed as (Eqs. 7–9).

$$B_D^2 = [f_t^{3 \times 3} (\text{CB} (D_r (B_D^1)))] \odot [\text{RAAM} (B_E^3)] \odot [f_t^{3 \times 3} (\text{RAAM} (B_E^4))] \quad (7)$$

$$B_D^3 = [f_t^{3 \times 3} (\text{CB} (D_r (B_D^2)))] \odot [\text{RAAM} (B_E^2)] \odot [f_t^{3 \times 3} (\text{RAAM} (B_E^3))] \quad (8)$$

$$B_D^4 = [f_t^{3 \times 3} (\text{CB} (D_r (B_D^3)))] \odot [\text{RAAM} (B_E^1)] \odot [f_t^{3 \times 3} (\text{RAAM} (B_E^2))] \quad (9)$$

The final predicted mask of the proposed EUIS-Net is computed in (Eq.10).

$$P_{mask} = \sigma (f^{1 \times 1} (B_D^4)) \quad (10)$$

Where $f^{1 \times 1}$ is the convolutional operation with a kernel size (1×1) and σ is the sigmoid operation.

2.1 Region Aware Attention Module

The region-aware attention module [16] employs a composite pooling strategy, which combines maximum and average pooling in a cascade to learn region-aware features, as shown in (Fig. 2-(a)). This is achieved by promoting region-wise important information during the forward pass and ensuring region-dependent flow during back-propagation. The proposed approach effectively discriminates foreground pixels from background pixels by maximising the value resulting from the combined use of average and max pooling features. The computational steps involved in RAAM are briefly described in this section. Let x be the input tensor of the model. The intermediate outputs (I_1, I_2) of the RAAM module are computed as (Eqs. 11–12)

$$I_1 = M_p (\text{GAP} (\Re (B_n (f^{3 \times 3} (x))))) \quad (11)$$

$$I_2 = \text{GAP} (M_p (\Re (B_n (f^{3 \times 3} (x))))) \quad (12)$$

where GAP is the global average pooling. The final output (y) of the RAAM module is then computed by Eq. 13.

$$y = \text{CCA} (\Re (B_n (f^{3 \times 3} (x)))) \times I_1 \times I_2 \times x \quad (13)$$

where CCA is the cross channel averaging operation.

2.2 Channel and Spatial Attention Module

In our network, spatial and channel attention mechanisms are integrated within a residual block (Fig. 2-(b)). The interstitial association of features is employed to generate the spatial attention map, which focusses on the 'where' aspect of the input data. In contrast, channel attention serves as an informative component that complements spatial attention by focussing on the 'what' aspect. This combination enhances the ability of the network to selectively emphasise significant features both spatially and across channels. The output of the channel attention output is denoted by (C_A) and is computed as given in (Eq. 14).

$$C_A = E_3 \otimes f^{3 \times 3} \left(\Re \left(f^{3 \times 3} [\text{GAP}(E_3) \oplus \text{GMP}(E_3)] \right) \right) \quad (14)$$

Where \otimes is point-wise multiplication and \oplus is the addition operator. GAP and GMP are the global average pooling and global max pooling operations, respectively.

The spatial attention output is denoted by (S_A) and computed as given in (Eq. 15).

$$S_A = C_A \otimes \Re \left(f^{3 \times 3} (C_p(C_A)) \right) \quad (15)$$

Where C_p is the channel pooling operation. Once the feature information is extracted and refined from the encoder blocks and attention mechanisms this information is fed to the decoder blocks to reconstruct the feature maps and restore the spatial dimensions to the given input.

3 Results and Discussion

3.1 Datasets

The proposed EUIS-Net model was evaluated in two challenging benchmark ultrasound imaging datasets (Table 1), namely BUSI [25] for the segmentation of breast cancer and DDTI [26] for the segmentation of thyroid nodules. Both datasets are publicly available and provide GT masks for the evaluation of image segmentation methods. Performance evaluation was performed using a five-fold cross-validation method due to the unavailability of a separate test set.

3.2 Evaluation Criteria

The segmentation performance of EUIS-Net was evaluated and compared with SOTA methods using several metrics, including the Jaccard index (J , equal to IoU), Dice similarity coefficient (D), accuracy (A_{cc}), sensitivity (S_n), and specificity (S_p). These metrics were calculated according to their definitions:

$$J = \frac{T_P}{T_P + F_P + F_N}, \quad (16)$$

$$D = \frac{2 \times T_P}{2 \times T_P + F_P + F_N}, \quad (17)$$

$$A_{cc} = \frac{T_P + T_N}{T_P + T_N + F_P + F_N}, \quad (18)$$

$$S_n = \frac{T_P}{T_P + F_N}, \quad (19)$$

$$S_p = \frac{T_N}{T_N + F_P}, \quad (20)$$

where T_P , T_N , F_P , and F_N denote the number of true positives, true negatives, false positives, and false negatives, respectively.

Dataset	Reference	Image Format	Original Resolution	Image Count	Resized to	Dataset Split	Classes	Task / Additional Info
BUSI	[25]	.png	$\sim 500 \times 500$	780	256×256	80%:10%:10%	3	Breast ultrasound segmentation, age 25-75
DDTI	[25]	.png	$560 \times 360, 280 \times 360, 245 \times 360$	637	256×256	80%:10%:10%	2	Thyroid nodule segmentation

Table 1: Details of the ultrasound image datasets used for the proposed EUIS-Net evaluation.

3.3 Experimental Setup

For model training, the images (Table 1) were augmented using contrast adjustments (with factors of $[\times 0.9, \times 1.1]$) and flipping operations (both in horizontal and vertical directions), which increased the size of the datasets by a factor of 5. The Adam optimiser was used with a maximum of 60 iterations and an initial learning rate of 0.001. In the absence of performance improvement on the validation set after five epochs, the learning rate was reduced by a quarter. To stop overfitting, an early stop strategy was implemented. The models were implemented through Keras using TensorFlow as the back-end and trained on an NVIDIA GTX 3090 GPU.

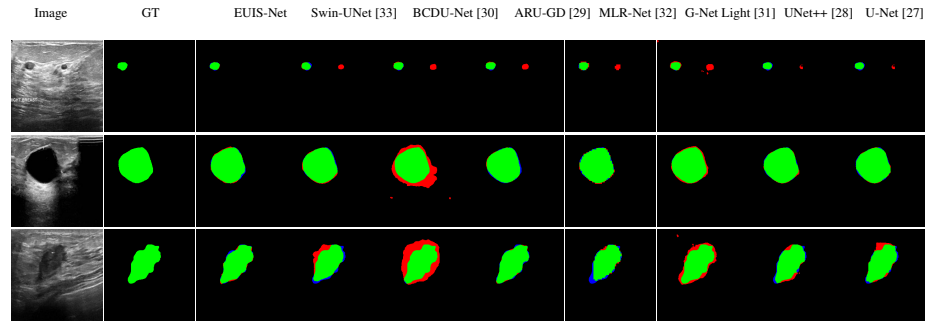


Fig. 3: Visual performance comparison of the proposed EUIS-Net on BUSI [25] dataset.

Method	Performance (%)				
	J	D	A_{cc}	S_n	S_p
U-Net [27]	67.77 \pm 2.35	76.96 \pm 3.67	95.48 \pm 3.60	78.33 \pm 4.35	96.13 \pm 2.07
UNet++ [28]	76.85 \pm 3.13	76.22 \pm 3.59	97.97 \pm 1.93	78.61 \pm 3.27	98.86 \pm 2.23
ARU-GD [29]	77.07 \pm 2.96	83.64 \pm 2.53	97.94 \pm 1.32	83.80 \pm 1.87	98.78 \pm 2.59
BCDU-Net [30]	74.49 \pm 3.65	66.75 \pm 2.31	94.82 \pm 1.28	86.85 \pm 3.95	95.57 \pm 2.72
G-Net Light [31]	75.97 \pm 3.81	83.97 \pm 2.20	96.22 \pm 2.85	83.45 \pm 2.28	97.11 \pm 3.80
MLR-Net [32]	76.09 \pm 2.04	83.67 \pm 3.06	96.65 \pm 2.55	84.39 \pm 1.13	98.04 \pm 1.44
Swin-UNet [33]	77.16 \pm 2.85	84.45 \pm 2.54	97.55 \pm 2.77	84.81 \pm 3.99	98.34 \pm 2.50
RA-Net [16]	77.48 \pm 2.08	84.68 \pm 2.91	97.82 \pm 1.92	85.37 \pm 3.32	98.14 \pm 1.95
Proposed EUIS-Net	78.12\pm1.85	85.42\pm2.13	98.04\pm1.10	87.93\pm1.02	98.72\pm1.26

Table 2: Performance (mean \pm std) comparison of EUIS-Net model with various SOTA methods on the breast lesion segmentation dataset BUSI [25].

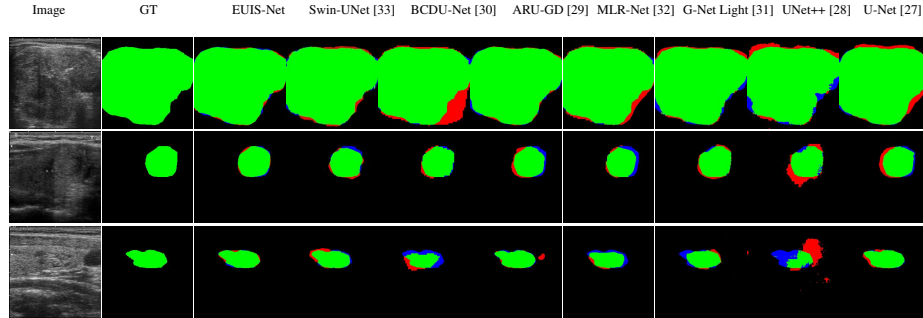


Fig. 4: Visual performance comparison of the proposed EUIS-Net on DDTI [26] dataset.

Method	Performance (%)				
	J	D	A_{cc}	S_n	S_p
U-Net [27]	74.76 \pm 1.36	84.08 \pm 3.19	96.55 \pm 2.48	85.50 \pm 3.09	97.57 \pm 1.61
UNet++ [28]	74.76 \pm 3.46	84.08 \pm 2.27	96.55 \pm 2.51	85.50 \pm 3.39	97.57 \pm 1.34
BCDU-Net [30]	77.79 \pm 1.90	79.49 \pm 2.27	93.22 \pm 2.51	82.31 \pm 3.39	94.34 \pm 1.34
ARU-GD [29]	77.07 \pm 1.90	83.64 \pm 2.56	97.94 \pm 2.55	83.80 \pm 4.20	98.78 \pm 2.35
G-Net Light [31]	80.76 \pm 2.42	85.59 \pm 1.80	97.79 \pm 2.65	85.23 \pm 3.74	98.98 \pm 2.01
MLR-Net [32]	82.66 \pm 2.14	85.72 \pm 1.02	97.91 \pm 2.60	79.54 \pm 4.28	98.82 \pm 2.18
Swin U-Net [33]	83.44 \pm 2.49	86.86 \pm 2.45	96.93 \pm 2.18	86.42 \pm 2.39	97.98 \pm 2.05
RA-Net [16]	83.43 \pm 1.87	86.01 \pm 1.78	97.98 \pm 2.30	82.21 \pm 3.07	98.88 \pm 1.13
Proposed EUIS-Net	84.73\pm1.19	89.01\pm1.01	98.15\pm1.24	88.13\pm1.18	99.05\pm1.03

Table 3: Performance (mean \pm std) comparison of EUIS-Net with various SOTA methods on the thyroid nodule segmentation dataset DDTI [26].

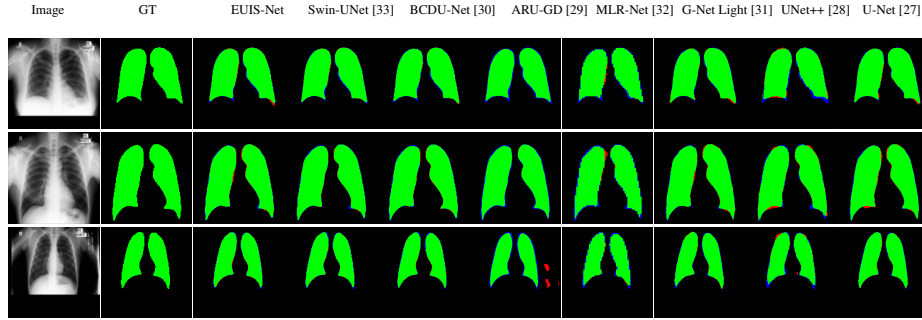


Fig. 5: Visual performance comparison of the proposed EUIS-Net on MC [34] dataset.

Method	Performance (%)				
	J	D	A_{cc}	S_n	S_p
U-Net [27]	94.38 \pm 2.10	97.10 \pm 1.58	98.53 \pm 1.18	95.99 \pm 2.04	99.40 \pm 0.44
UNet++ [28]	94.57 \pm 2.82	97.20 \pm 1.82	98.59 \pm 1.20	96.28 \pm 2.03	99.36 \pm 0.62
ARU-GD [29]	94.65 \pm 2.35	97.25 \pm 1.48	98.62 \pm 1.30	95.97 \pm 1.77	99.50\pm0.48
BCDU-Net [30]	94.53 \pm 2.59	97.19 \pm 1.57	98.57 \pm 1.20	96.00 \pm 1.11	99.43 \pm 0.32
G-Net Light [31]	94.47 \pm 2.84	97.22 \pm 1.31	98.03 \pm 1.69	95.09 \pm 1.55	99.42 \pm 0.48
MLR-Net [32]	94.80 \pm 2.29	97.34 \pm 1.85	98.70 \pm 0.70	95.57 \pm 1.68	99.02 \pm 0.85
Swin-UNet [33]	90.69 \pm 1.40	95.07 \pm 1.62	97.61 \pm 0.65	94.34 \pm 1.39	98.65 \pm 0.59
RA-Net [16]	94.88 \pm 1.80	97.49 \pm 1.28	98.87 \pm 0.21	96.89 \pm 1.67	99.20 \pm 0.40
Proposed EUIS-Net	96.49\pm1.59	98.21\pm1.09	99.14\pm0.14	98.40\pm1.05	99.33\pm0.11

Table 4: Performance (mean \pm std) comparison of the proposed EUIS-Net with various SOTA methods for chest X-ray image segmentation on the MC [34] dataset.

3.4 Comparisons with SOTA Methods

For both data sets (Table 1) we compared EUIS-Net with eight state-of-the-art medical image segmentation methods, including ARU-GD [29], BCDU-Net [30], G-Net Light [31], MLR-Net [32], RA-Net [16], Swin-Unet [33], U-Net [27] and UNet++ [28].

Table 2 presents the statistical comparison of the proposed EUIS-Net with the other methods. Compared to other methods, the Jaccard index (J) of the proposed EUIS-Net is improved by 0.64%, .96%, 2.03%, 2.15%, 3.63%, 1.05%, 1.27%, and 10.35% than RA-Net [16], Swin-Unet [33], MLR-Net [32], G-Net Light [31], BCDU-Net [30], ARU-GD [29], UNet++ [28], and U-Net [27], respectively on the BUSI dataset [25]. Figure 3 presents the visual results of different challenges in the segmentation of breast cancer. The proposed EUIS-Net achieved the best segmentation results, which closely resemble GT data, even for breast cancer images with varying sizes and irregular shapes. Table 3 presents the statistical comparison of the proposed EUIS-Net with the other methods. Compared to other methods, the Jaccard index (J) of the proposed EUIS-Net is improved by 1.3%, 1.29%, 2.07%, 3.97%, 7.66%, 6.94%, 9.97%, and 10.67% than RA-Net [16], Swin-Unet [33], MLR-Net [32], G-Net Light [31], BCDU-Net [30],

ARU-GD [29], UNet++ [28], and U-Net [27], respectively on the DDTI dataset [26] for thyroid nodule segmentation. Figure 4 presents the visual results of different challenges in the segmentation of breast cancer. The proposed EUIS-Net achieved the best segmentation results, which closely resemble GT data, even for thyroid nodule images with varying sizes and irregular shapes.

The generalisation of the proposed EUIS-Net is evaluated on the MC [34] data set for chest X-ray image segmentation. Table 4 presents the statistical comparison of the proposed EUIS-Net with the other methods. Compared to other methods, the Jaccard index (J) of the proposed EUIS-Net is improved by 1.3%, 1.29%, 2.07%, 3.97%, 7.66%, 6.94%, 9.97%, and 10.67% than RA-Net [16], Swin-Unet [33], MLR-Net [32], G-Net Light [31], BCDU-Net [30], ARU-GD [29], UNet++ [28], and U-Net [27], respectively on the MC dataset [34] for chest X-ray segmentation. Figure 5 presents the visual results of different chest X-ray image segmentation challenges. The proposed EUIS-Net achieved the best segmentation results, which closely resemble GT data.

4 Conclusions

We have developed EUIS-Net, a novel and effective methodology for segmenting ultrasound images with precision, aimed at overcoming challenges like inherent noise and unpredictability of ultrasound images. To address these challenges, we proposed EUIS-Net, a CNN network designed to segment ultrasound images efficiently and precisely. The proposed EUIS-Net uses four encoder-decoder blocks, resulting in a notable decrease in computational complexity while achieving excellent performance. The proposed EUIS-Net integrates both channel and spatial attention mechanisms into the bottleneck to improve feature representation and collect significant contextual information. In addition, EUIS-Net incorporates a region-aware attention module (RAAM) into the skip connections, which enhances the ability to concentrate on lesion regions. When evaluated on two publicly available benchmark ultrasound image datasets, EUIS-Net outperformed a variety of recent methods. Despite its exceptional performance, we have identified areas for further improvement. We suggest employing EUIS-Net in a semi-supervised manner to reduce data requirements for training. EUIS-Net is suitable not only for immediate medical imaging applications in ultrasound image segmentation but also holds promise for adaptation and expansion to other medical imaging and segmentation tasks.

References

1. “Breast Cancer, accessed on: Jul 08, 2024.” [Online]. Available: <https://www.who.int/news/item>
2. F. Islami, K. D. Miller, R. L. Siegel, Z. Zheng, J. Zhao, X. Han, J. Ma, A. Jemal, and K. R. Yabroff, “National and state estimates of lost earnings from cancer deaths in the United States,” *JAMA oncology*, vol. 5, no. 9, pp. e191 460–e191 460, 2019.
3. W. H. Organization, *Global breast cancer initiative implementation framework: assessing, strengthening and scaling-up of services for the early detection and management of breast cancer*. World Health Organization, 2023.

4. P. Skaane, A. I. Bandos, L. T. Niklason, S. Sebuødegård, B. H. Østerås, R. Gullien, D. Gur, and S. Hofvind, "Digital mammography versus digital mammography plus tomosynthesis in breast cancer screening: the oslo tomosynthesis screening trial," *Radiology*, vol. 291, no. 1, pp. 23–30, 2019.
5. G. Carlino, P. Rinaldi, M. Giuliani *et al.*, "Ultrasound-guided preoperative localization of breast lesions: a good choice. *j ultrasound* 22: 85–94," 2019.
6. T. M. Khan and A. Robles-Kelly, "Machine learning: Quantum vs classical," *IEEE Access*, vol. 8, pp. 219 275–219 294, 2020.
7. S. Iqbal, T. M. Khan, K. Naveed, S. S. Naqvi, and S. J. Nawaz, "Recent trends and advances in fundus image analysis: A review," *Computers in Biology and Medicine*, vol. 151, p. 106277, 2022.
8. T. M. Khan, S. S. Naqvi, A. Robles-Kelly, and I. Razzak, "Retinal vessel segmentation via a multi-resolution contextual network and adversarial learning," *Neural Networks*, vol. 165, pp. 310–320, 2023.
9. T. M. Khan, M. Arsalan, S. Iqbal, I. Razzak, and E. Meijering, "Feature enhancer segmentation network (fes-net) for vessel segmentation," in *2023 International Conference on Digital Image Computing: Techniques and Applications (DICTA)*. IEEE, 2023, pp. 160–167.
10. S. Iqbal, T. M. Khan, S. S. Naqvi, A. Naveed, M. Usman, H. A. Khan, and I. Razzak, "Ldmres-net: A lightweight neural network for efficient medical image segmentation on iot and edge devices," *IEEE journal of biomedical and health informatics*, 2023.
11. H.-H. Chiang, J.-Z. Cheng, P.-K. Hung, C.-Y. Liu, C.-H. Chung, and C.-M. Chen, "Cell-based graph cut for segmentation of 2d/3d sonographic breast images," in *2010 IEEE International Symposium on Biomedical Imaging: From Nano to Macro*. IEEE, 2010, pp. 177–180.
12. M. Xian, Y. Zhang, and H.-D. Cheng, "Fully automatic segmentation of breast ultrasound images based on breast characteristics in space and frequency domains," *Pattern Recognition*, vol. 48, no. 2, pp. 485–497, 2015.
13. A. Madabhushi and D. N. Metaxas, "Combining low-, high-level and empirical domain knowledge for automated segmentation of ultrasonic breast lesions," *IEEE transactions on medical imaging*, vol. 22, no. 2, pp. 155–169, 2003.
14. J. Shan, H. Cheng, and Y. Wang, "Completely automated segmentation approach for breast ultrasound images using multiple-domain features," *Ultrasound in medicine & biology*, vol. 38, no. 2, pp. 262–275, 2012.
15. T. M. Khan, S. S. Naqvi, and E. Meijering, "Esdmr-net: A lightweight network with expand-squeeze and dual multiscale residual connections for medical image segmentation," *Engineering Applications of Artificial Intelligence*, vol. 133, p. 107995, 2024.
16. A. Naveed, S. S. Naqvi, S. Iqbal, I. Razzak, H. A. Khan, and T. M. Khan, "Ra-net: Region-aware attention network for skin lesion segmentation," *Cognitive Computation*, pp. 1–18, 2024.
17. T. M. Khan, S. S. Naqvi, and E. Meijering, "Leveraging image complexity in macro-level neural network design for medical image segmentation," *Scientific Reports*, vol. 12, no. 1, p. 22286, 2022.
18. S. Javed, T. M. Khan, A. Qayyum, A. Sowmya, and I. Razzak, "Advancing medical image segmentation with mini-net: A lightweight solution tailored for efficient segmentation of medical images," *arXiv preprint arXiv:2405.17520*, 2024.
19. M. Matloob Abbasi, S. Iqbal, K. Aurangzeb, M. Alhussein, and T. M. Khan, "Lmbis-net: A lightweight bidirectional skip connection based multipath cnn for retinal blood vessel segmentation," *Scientific Reports*, vol. 14, no. 1, p. 15219, 2024.
20. T. M. Khan, S. Iqbal, S. S. Naqvi, I. Razzak, and E. Meijering, "Lmbf-net: A lightweight multipath bidirectional focal attention network for multifeatures segmentation," *arXiv preprint arXiv:2407.02871*, 2024.

21. B. Shareef, A. Vakanski, P. E. Freer, and M. Xian, "Estan: Enhanced small tumor-aware network for breast ultrasound image segmentation," in *Healthcare*, vol. 10, no. 11, 2022, p. 2262.
22. N. S. Punna and S. Agarwal, "Rca-iunet: a residual cross-spatial attention-guided inception u-net model for tumor segmentation in breast ultrasound imaging," *Machine Vision and Applications*, vol. 33, no. 2, p. 27, 2022.
23. K. Yang, A. Suzuki, J. Ye, H. Nosato, A. Izumori, and H. Sakanashi, "Ctg-net: Cross-task guided network for breast ultrasound diagnosis," *PloS one*, vol. 17, no. 8, p. e0271106, 2022.
24. Y. Wu, R. Zhang, L. Zhu, W. Wang, S. Wang, H. Xie, G. Cheng, F. L. Wang, X. He, and H. Zhang, "Bgm-net: boundary-guided multiscale network for breast lesion segmentation in ultrasound," *Frontiers in Molecular Biosciences*, vol. 8, p. 698334, 2021.
25. W. Al-Dhabyani, M. Gomaa, H. Khaled, and A. Fahmy, "Dataset of breast ultrasound images," *Data in brief*, vol. 28, p. 104863, 2020.
26. ———, "Dataset of breast ultrasound images," *Data in Brief*, vol. 28, p. 104863, 2020.
27. O. Ronneberger, P. Fischer, and T. Brox, "U-net: Convolutional networks for biomedical image segmentation," in *Medical Image Computing and Computer-Assisted Intervention—MICCAI 2015: 18th International Conference, Munich, Germany, October 5-9, 2015, Proceedings, Part III* 18. Springer, 2015, pp. 234–241.
28. Z. Zhou, M. M. Rahman Siddiquee, N. Tajbakhsh, and J. Liang, "Unet++: A nested U-Net architecture for medical image segmentation," in *Deep Learning in Medical Image Analysis (DLMIA) & Multimodal Learning for Clinical Decision Support (ML-CDS) Held in Conjunction with MICCAI*, 2018, pp. 3–11.
29. D. Maji, P. Sigedra, and M. Singh, "Attention Res-UNet with Guided Decoder for semantic segmentation of brain tumors," *Biomedical Signal Processing and Control*, vol. 71, p. 103077, 2022.
30. R. Azad, M. Asadi-Aghbolaghi, M. Fathy, and S. Escalera, "Bi-directional ConvLSTM U-Net with densely connected convolutions," in *IEEE/CVF International Conference on Computer Vision (ICCV) Workshops*, 2019.
31. S. Iqbal, S. Naqvi, H. Ahmed, A. Saadat, and T. M. Khan, "G-net light: A lightweight modified google net for retinal vessel segmentation," in *Photonics*, vol. 9, no. 12. MDPI, 2022, pp. 923–936.
32. S. Iqbal, T. M. Khan, S. S. Naqvi, and G. Holmes, "MLR-Net: A multi-layer residual convolutional neural network for leather defect segmentation," *Engineering Applications of Artificial Intelligence*, vol. 126, p. 107007, 2023.
33. H. Cao, Y. Wang, J. Chen, D. Jiang, X. Zhang, Q. Tian, and M. Wang, "Swin-Unet: Unet-like pure transformer for medical image segmentation," in *European Conference on Computer Vision (ECCV) Workshops*, 2023, pp. 205–218.
34. S. Jaeger, S. Candemir, S. Antani, Y.-X. J. Wang, P.-X. Lu, and G. Thoma, "Two public chest X-ray datasets for computer-aided screening of pulmonary diseases," *Quantitative Imaging in Medicine and Surgery*, vol. 4, no. 6, p. 475, 2014.